Discrete dislocation simulations and size dependent hardening in single slip

H. Cleveringa, E. Van der Giessen and A. Needleman*

Delft University of Technology, Department of Mechanical Engineering, Mekelweg 2, 2628 CD Delft, the Netherlands
* Brown University, Division of Engineering, Box D, Providence RI 02912, U.S.A.

Abstract. Plastic deformation in two-dimensional monophase and composite materials is studied using a discrete dislocation dynamics method. In this method, dislocations are represented by line defects in a linear elastic medium, and their interactions with boundaries or second-phase elastic particles are incorporated through a complementary finite element solution. The formulation includes a set of simple constitutive rules to model the lattice resistance to dislocation glide, as well as the generation, annihilation and pinning of dislocations at point obstacles. The focus is on the predicted strain hardening of these materials when only a single slip system is active. When the particle morphology is such as to require geometrically necessary dislocations, hardening in the composite materials exhibits a distinct size effect. This size effect is weaker than that predicted by simple analytical estimates based on geometrically necessary dislocations.

1 INTRODUCTION

The plastic flow properties of metal-matrix composite materials have been predicted either within dislocation approaches, e.g. [1, 2, 3], or continuum plasticity approaches, e.g. [4]. Traditional dislocation approaches postulate a dislocation mechanism and then investigate the consequences of the assumed mechanism for the mechanical response of the composite. The continuum analyses are based on solving boundary problems for multi-phase solids, with each phase characterized as a classical elastic-plastic (or elastic) material.

There are significant limitations to both of these approaches. Classical continuum analyses presume a size independent response, whereas a definite size dependence is seen for composites with reinforcements in the 1 to 100 μm range. Presuming a dislocation structure avoids the issue of what dislocation structures evolve for a given composite morphology and loading history.

In this paper, we discuss predictions of the stress-strain response of a simple model composite material that are obtained using a discrete dislocation framework in which plastic flow arises directly from the collective motion of large numbers of discrete dislocations, [5, 6, 7]. The plastic stress-strain response and the evolution of the dislocation structure are outcomes of the boundary value problem solution. For comparison purposes, we also discuss corresponding predictions for a homogeneous material in order to get some insight into the separate roles of dislocation interactions and the interactions with the elastic particles. The focus is on the dependence of the plastic flow behavior on the reinforcement size.

2 FORMULATION

The deformation of a linear elastic body with a distribution of dislocations is considered. The elastic properties of the body need not be homogeneous. As described in detail in [6] and [7], the deformation history is calculated in an incremental manner, with each time step involving three main computational stages: (i) determining the current stress and strain state for the current dislocation arrangement; (ii) determining the forces between dislocations, i.e. the Peach-Koehler force; and (iii)

determining the rate of change of the dislocation structure, which involves the motion of dislocations, the generation of new dislocations, their mutual annihilation, and their pinning at obstacles.

The key idea for determining the current state of the body with the current dislocation distribution (see also [8]) is that, in the current state, the displacement, strain and stress fields are written as the superposition of two fields,

$$\boldsymbol{u} = \tilde{\boldsymbol{u}} + \hat{\boldsymbol{u}}, \quad \boldsymbol{\varepsilon} = \tilde{\boldsymbol{\varepsilon}} + \hat{\boldsymbol{\varepsilon}}, \quad \boldsymbol{\sigma} = \tilde{\boldsymbol{\sigma}} + \hat{\boldsymbol{\sigma}} \tag{1}$$

respectively. The (˜) fields are the superposition of the fields of the individual dislocations, in their current configuration, but in an infinite medium of the homogeneous matrix material, and are obtained by superposition of the fields $(\boldsymbol{u}^i, \boldsymbol{\varepsilon}^i, \boldsymbol{\sigma}^i)$ associated with the individual dislocations (see e.g. [9, 10]),

$$\tilde{\boldsymbol{u}} = \sum_i \boldsymbol{u}^i, \quad \tilde{\boldsymbol{\varepsilon}} = \sum_i \boldsymbol{\varepsilon}^i, \quad \tilde{\boldsymbol{\sigma}} = \sum_i \boldsymbol{\sigma}^i \quad (i = 1, \dots, n) \tag{2}$$

where n is the number of dislocations in the current configuration. The (ˆ) fields represent the image fields that correct for the actual boundary conditions and for any elastic heterogeneity. A key point is that the (ˆ) fields are smooth, so that the boundary value problem for them can be conveniently solved by the finite element method (or some other numerical method, e.g., the boundary element method).

The smoothness of the (ˆ) fields is illustrated in Fig. 1. Figure 1a shows the finite element visualization of the total dispacement field for a model plane strain composite material that is being sheared parallel to its single slip plane (for more details, see Sec. 4). The highly localized deformation pattern that ensues is evident in this figure. The corresponding $\hat{\boldsymbol{u}}$ field, which has rather diffuse gradients and can be resolved even with a rather coarse mesh, is shown in Fig. 1b. The difference between these fields, i.e. $\boldsymbol{u} - \hat{\boldsymbol{u}}$, is the displacement field due to the discrete dislocations, $\tilde{\boldsymbol{u}}$. The highly localized displacement pattern in Fig. 1a stems entirely from the discrete dislocation fields. Hence, the fact that the deformations in Fig. 1a are concentrated in a row of elements does not indicate a mesh dependence of the results, as would be the case for localized deformations in a rate independent strain softening continuum.

Edge dislocations, all having the same Burgers vector magnitude, b, are considered on a single slip system, with the slip plane normal $\boldsymbol{n}$ being in the x_2-direction and with the glide direction $\boldsymbol{m}$ being in the x_1-direction. The component of the Peach-Koehler force f^i on dislocation i in the glide direction is determined by the local stress state as $f^i = b^i \tau^i$ with $\tau^i = \boldsymbol{m} \cdot (\hat{\boldsymbol{\sigma}} + \sum_{j \neq i} \boldsymbol{\sigma}^j) \cdot \boldsymbol{n}$ being the resolved shear stress. The magnitude of the glide velocity v^i of dislocation i is taken to be linearly related to the Peach-Koehler force f^i through the drag relation $f^i = Bv^i$. Obstacles to dislocation motion are modeled as fixed points on a slip plane. Such obstacles account for the effects of small precipitates or for dislocations on other, secondary, slip systems in blocking slip on the primary slip plane. Pinned dislocations can only pass the obstacles when their Peach-Koehler force exceeds an obstacle dependent value $\tau_{\mathrm{obs}}b$. Annihilation of two dislocations with opposite Burgers vector occurs when they are sufficiently close together within a material-dependent, critical annihilation distance L_e. This distance is here chosen to be $6b$ [11]. New dislocation pairs are generated by simulating Frank-Read sources. In two dimensions, with single slip, this is simulated by point sources on the slip plane which generate a dislocation dipole when the magnitude of the Peach-Koehler force at the source exceeds the critical value $\tau_{\mathrm{nuc}}b$ during a period of time t_{nuc}. The distance L_{nuc} between the two new dislocations is specified as

$$L_{\mathrm{nuc}} = \frac{\mu}{2\pi(1-\nu)} \frac{b}{\tau_{\mathrm{nuc}}}, \tag{3}$$

with μ and ν the elastic shear modulus and Poisson's ratio, respectively. At this distance, the shear stress of one dislocation acting on the other is balanced by the slip plane shear stress. The magnitude of τ_{nuc} is randomly chosen from a Gaussian distribution with mean strength $\bar{\tau}_{\mathrm{nuc}}$.
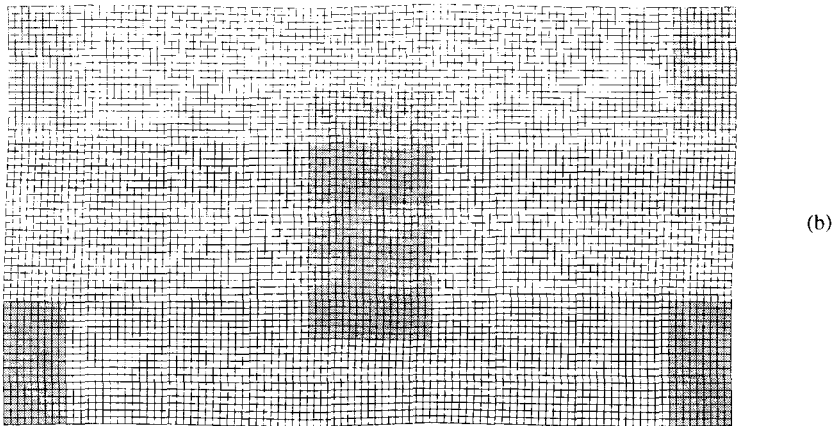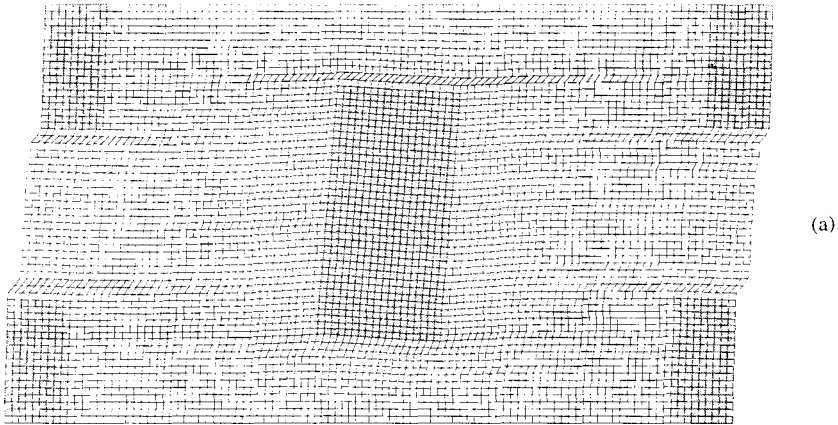
Figure 1: Displacement fields visualized by distorted finite element meshes for a unit cell of a particle reinforced model material sheared to a shear strain of 1 % (the grey regions indicate the particles). (a) total displacement field $\tilde{u} + \hat{u}$; (b) image field $\hat{u}$. All displacements are amplified by a factor 10.

More complete descriptions of the formulation are presented in [6, 7]. It is worth emphasizing that the formulation is a full three-dimensional one, although to date only two-dimensional plane strain problems have been solved. Specifically, the calculations to be discussed are carried out for monophase or composite materials arranged as a doubly periodic array of rectangular cells. Each phase has isotropic elastic moduli. The unit cell (size $2w \times 2h$) is subjected to plane strain, simple shear, which is prescribed through displacement boundary conditions at the top and bottom of the cell, $x_2 = \pm h$. The average shear stress required to sustain the shear strain Γ is denoted by $\bar{\tau}$.

3   MONOPHASE MATERIAL RESULTS

Figure 2, from [6], shows predicted shear stress versus shear strain curves for a monophase material when the source density ρ_{nuc} is varied and including, as a limiting situation, a case where there are no active dislocation sources. Stresses are normalized by the elastic shear modulus μ. Due to the presence of initial mobile dislocations, there is no elastic regime. The simulations exhibit two characteristic strength levels: the *yield strength* corresponding to the peak in the stress-strain
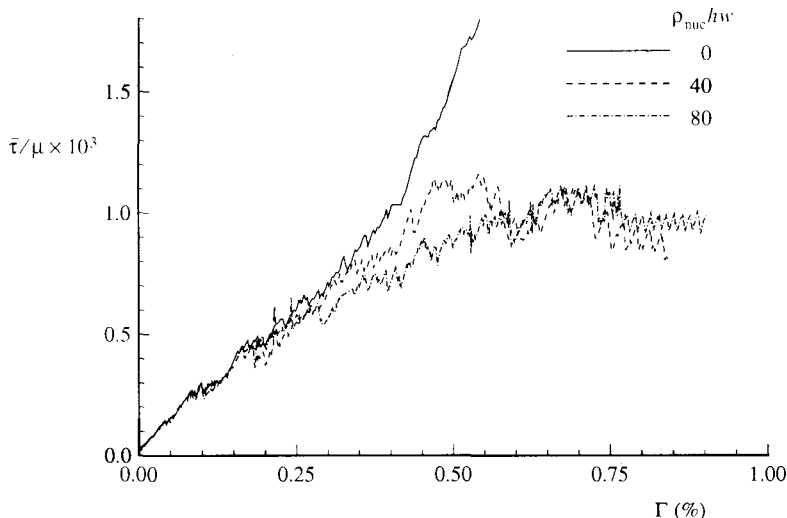
Figure 2: Overall shear stress ($\bar{\tau}$) response to simple shear (Γ) of a monophase material containing initial mobile dislocations and obstacles, for varying densities ρ_{nuc} of dislocation sources.

curve, and the (lower) *flow strength* at which the material continues to deform steadily. The latter is associated with the localization of dislocation activity on a few isolated slip planes. The simulated behavior in Fig. 2 is essentially annihilation controlled until $\Gamma \approx 0.25\,\%$, because the dislocation density is independent of the source density in that range. Beyond that strain level, all remaining dislocations tend to be removed by annihilation if there are no sources, and the response tends to become purely elastic. If there are sufficient sources, dislocation generation wins out over annihilation at some point. The rate of dislocation nucleation then appears to be virtually independent of the source density, and controlled by the strength of the sources. The source density has some effect on the hardening behavior and the yield strain, but is seemingly unimportant for the yield strength and for the flow strength.

The effect of obstacle density on the stress-strain response is shown in Fig. 3, also from [6]. The initial mobile dislocation density is the same as for the case in Fig. 2. The two cases with the lower obstacle density exhibit stress-strain responses that do not show a distinct yield point, but exhibit a more gradual transition to flow. In these cases, there is a more or less monotonic decrease of dislocation density until a steady-state value is reached. For the case with the highest density, $\rho_{\mathrm{obs}} = 320/hw$, there is relatively strong initial strain hardening, and a very sharp yield point. Annihilation is essentially inactive because, for the given initial (mobile) dislocation density of $\rho = 93/hw$, the obstacles effectively prevent dislocation motion over distances large enough for annihilation to become possible. The sharp yield point corresponds to a peak in the mobile dislocation density. The strain regime just after the stress drop is characterized by a very high annihilation–generation activity that continues until around $\Gamma = 0.7\,\%$, after which the dislocations seem to have found 'stable' positions, and the material hardens again.

4 COMPOSITE MATERIALS

Yield due to easy glide in materials with reinforcing elastic particles has similar charateristics as discussed above when the fraction of particles and their morphology is such that there are bands or veins of unreinforced matrix material [6, 7]. However, when the particles block all slip planes, as in the case of the morphology in Fig. 1 (shown also in the inset of Fig. 4), the behaviour is quite different. The simulations discussed in [7] show that such composites exhibit high strain hardening,
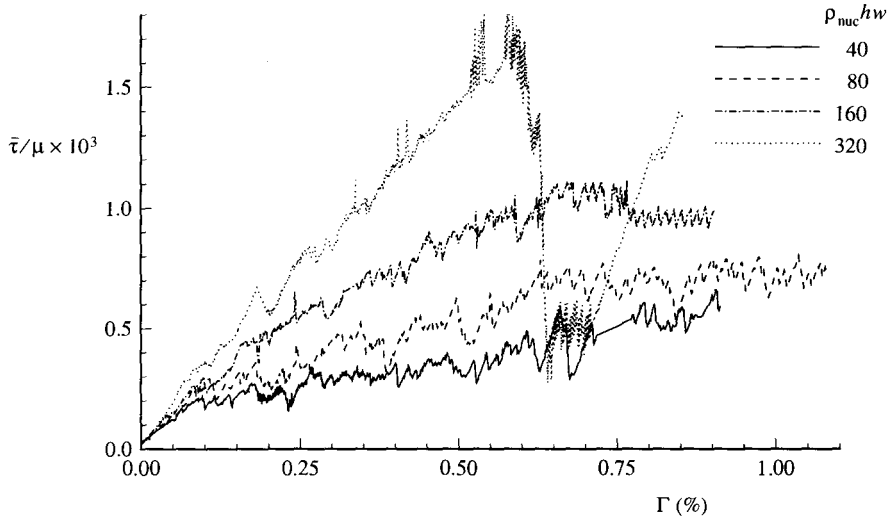
Figure 3: Effect of obstacle density on shear stress response in monophase material containing initial mobile dislocations and dislocation sources ($\rho_{\mathrm{nuc}} = 80/hw$).

which is dependent on the size of the particles. The size effect for this particular morphology is further explored here by systematically varying the size of the particles within the range from 0.5 to 2 times a reference particle size. The reference size is such that the half height h of the cell is equal to L, the latter being a fixed length scale set by the matrix material as $L = 4000b$. Thus, the reference particle height for particles with an aspect ratio of 2 and an area fraction of 20 % is $4700b$ (i.e. $1.2\,\mu$m if the matrix has a Burgers vector of $b = 2.5 \times 10^{-10}$ m.)

Figure 4 shows the shear stress vs shear strain responses for initially dislocation-free materials with three size scales of particles, specified by $h/L = 0.5$, 1 and 2. The random distributions of dislocation sources and obstacles for each of the three materials were so that the corresponding densities were roughly the same. The figure shows a systematic trend that the flow strength increases with decreasing particle size. This is confirmed by computations using different distributions of sources and obstacles, and by simulations for intermediate particle sizes; these results are not included in this figure to maintain clarity.

Snapshots of the dislocation distribution in the three materials at the same shear strain of around 1 % are displayed in Fig. 5. Upon comparing the three distributions (note that there is a factor of 16 difference in area between the smallest and largest cells), one observes an evident difference between the organization of dislocations for the three sizes. What appears to be of particular importance is the distinction between dislocation pile-ups against the particles versus the more or less random distribution in the matrix away from the particles. Piling-up of dislocations against the particle sides leads to the development of dislocation walls or tilt boundary like structures that are "geometrically necessary" to accomodate the particle rotation (see Fig. 1). Ashby's [1] treatment of geometrically necessary dislocations employs a similar model material as the one used in our simulations, and he concludes that the density of geometrically necessary dislocations increases linearly with strain, while additional dislocations are being generated in a statistical manner.

From the outcome of a dislocation evolution process as considered here, it is impossible to unambiguously identify which dislocations are geometrically necessary and which are statistically stored. In [7] we have adopted the working definition that all dislocations on either side of the central particle and within a distance of 0.1 times the particle spacing are termed geometrically necessary. It appears that the density (per unit length of the particle) of dislocations piling up against the central parti-
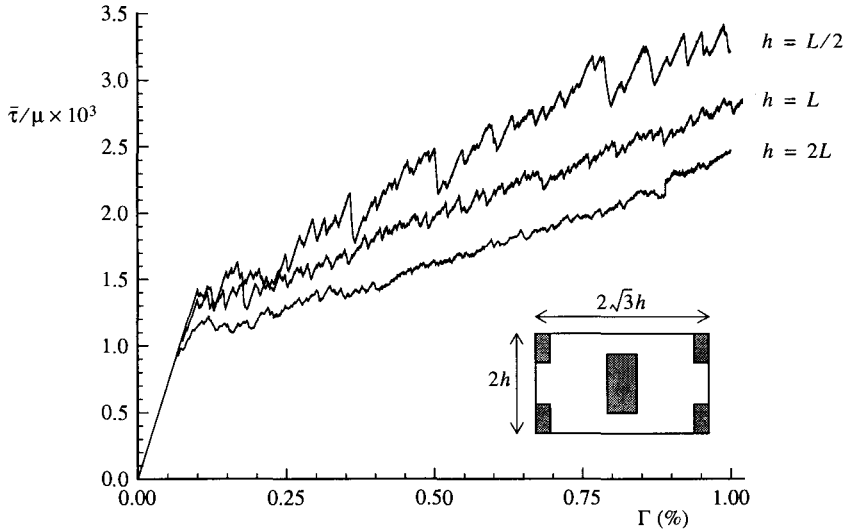
**Figure 4**: Shear stress response to simple shear of composite materials with various size scales of particles.

cle in Fig. 5 increases with increasing particle size. However, not all dislocations piling up against particles are geometrically necessary, as they may have arrived there as a consequence of the dynamics of dislocation motion, generation and pinning. Indeed, closer examination of the dislocation distribution in Fig. 5 for $h = 2L$ suggests that the density of dislocations near the interface between the central particle and the matrix is around 70 % larger than the density of geometrically necessary dislocations expected from the particle rotation at this strain. The lattice curvature and induced rotation due to these dislocations is compensated by a concentration of like-signed dislocations in the matrix at the other side of the particle. For the smaller particle size $(h = L/2)$ such an over-saturation of dislocation pile-ups is not observed, so that the above-mentioned working definition actually gives a fair identification of geometrically necessary dislocations. In this case, the ratio of geometrically necessary dislocations compared to the total ones remains roughly constant during the deformation process. Indeed, it is observed from the dislocation evolution shown in Fig. 6 that the total dislocation density and hence the density of geometrically necessary dislocations increases linearly with strain, as would be required by Ashby's [1] description. In fact, Fig. 6 shows that, over the strain range considered here, there is a linear increase of the total dislocation density with strain irrespective of particle size. The important effect of particle size appears to be reflected in the rate of dislocation evolution.

How are these dislocation structures responsible for the size effect seen in Fig. 4? A more detailed study of the predicted stress–strain curves in Fig. 4 and results for other realizations reveal that there is a reasonable correlation between particle size and the average tangent modulus $d\bar{\tau}/d\Gamma$. On the other hand, the initial yield stress varies within $0.5 \times 10^{-3}\mu$ in all the calculations here but with no correlation with reinforcement size. This is due to the fact that the initial yield stress is determined by the statistics of the location and strength of the dislocation sources. Apparently, the tangent modulus is to a much smaller extent determined by the statistics of the dislocation distribution, although it remains difficult to pin-point precisely how geometrically necessary dislocations are responsible for this.
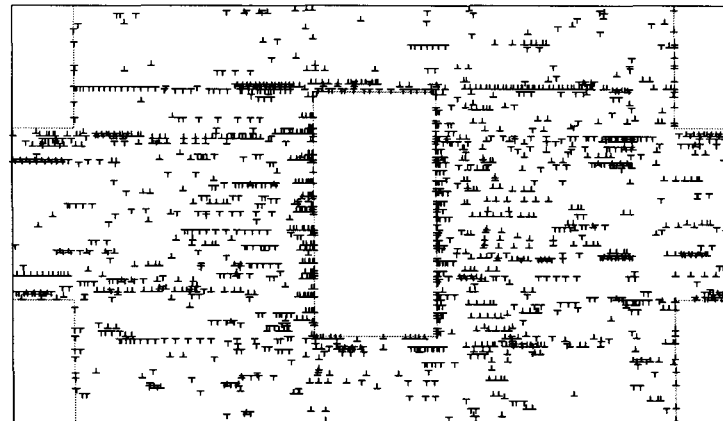
On average, the hardening for all sizes appears to be linear with strain (Fig. 4), so that the tangent modulus is fairly constant. Figure 7 summarizes the tangent moduli as a function of particle size, as obtained from the stress-strain curves in Fig. 4 as well as from other simulations using intermediate
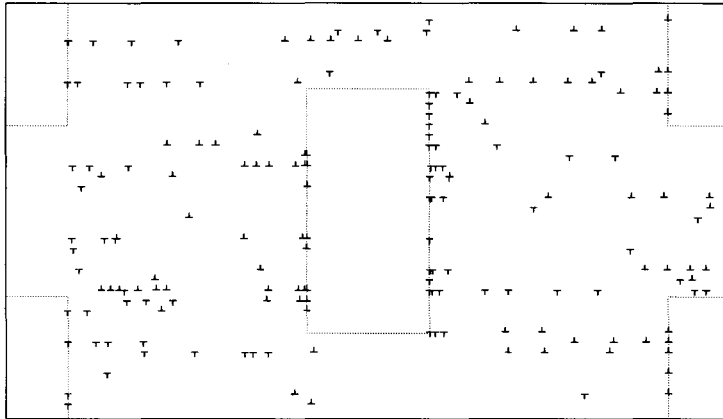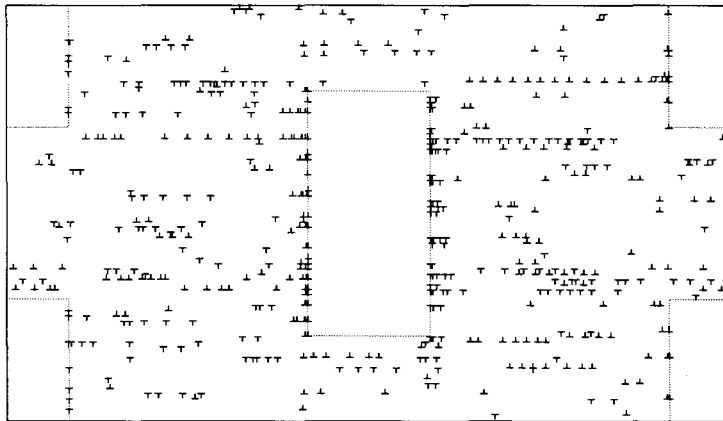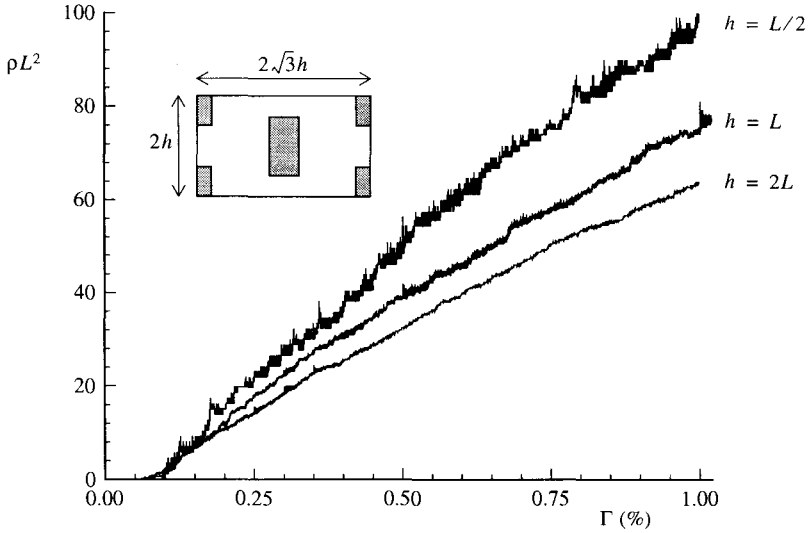
Figure 5: Dislocation distributions at $\Gamma \approx 1\%$ for three size scales of the reinforcing particles (cf. Fig 4). Note that the actual area of succesive unit cells differs by a factor of 4.

Figure 6: Evolution of the total (i.e. pinned and mobile) dislocations for three size scales of the reinforcing particles, corresponding to the stress-strain curves in Fig. 4.

particle sizes. For $h/L = 0.5$, the serrations in the stress-strain curve make it somewhat difficult to find a unique tangent modulus; therefore, three values are plotted that give an indication of the scatter. For h/L in between 0.5 and 1. it was not possible to use exactly the same density of sources and obstacles, so that the results of three simulations at slightly different h/L are included for which these densities vary within 25 % of the nominal value used. The distinct results for the sizes with $h/L \geq 1$ are from different simulations with the same source and obstacle density but with different random positions. Clearly, there is a substantial amount of variation in the results, which is due to the fact the unit cell used comprises only 2 particles. Nevertheless, the effect of particle size, through h/L, is persistent. Although the amount of data in Fig. 7 is too small to be statistically meaningful, it suggests that a size effect on hardening according to $d\bar{\tau}/d\Gamma \propto h^{-1/3}$ is reasonable. Also shown in Fig. 7 are the normalized dislocation densities for the various cases at $\Gamma = 1\%$. It is interesting to note that the dislocation density appears to scale in the same way: $\rho \propto h^{-1/3}$.

It is of some interest to confront these predictions with relatively simple size effect predictions based on the notion of geometrically necessary dislocations by Ashby [1]. He concludes that a shear deformation process like the one studied here is governed by the stress-strain relationship

$$\bar{\tau} = \bar{\tau}_0 + \beta\mu\sqrt{\frac{b\Gamma}{\lambda^G}} \qquad (4)$$

where λ^G is the spacing between particles. Furthermore, $\bar{\tau}_0$ is the initial flow stress of the matrix, and incorporates contributions to hardening not due to dislocations (e.g. solution hardening). The coefficient β is a geometric factor which has a value of approximately 0.35 [1, 2]. This relationship is based on the well-known assumption that the flow stress depends on the square root of the dislocation density, and assumes that the density of geometrically necessary dislocations, ρ^G, dominates. The expression (4) is obtained by invoking that ρ^G scales as [1]

$$\rho^G \propto \frac{\Gamma}{\lambda^G b}. \qquad (5)$$

Observing that the particle spacing λ^G scales directly with the size h of the unit cell in our simulations, these estimates would predict the following size effects: $\rho^G \propto h^{-1}$ and $d\bar{\tau}/d\Gamma \propto h^{-1/2}$. Clearly, the
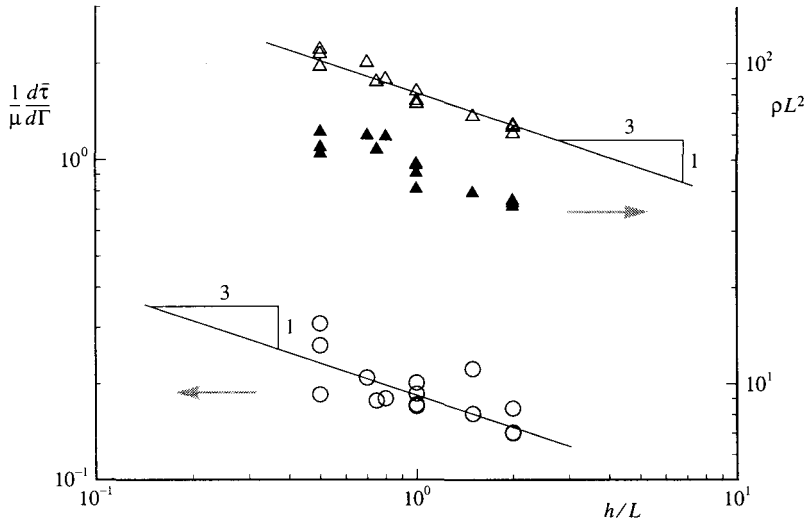
Figure 7: Effect of particle size, through h/L, on the average tangent modulus $d\bar{\tau}/d\Gamma$ (○) and the dislocation density (△: mobile and pinned dislocations; ▲: mobile dislocations; here, at $\Gamma = 1\%$).

results in Fig. 7 do not comply with these estimates, nor do we observe the parabolic hardening according to (4) in Fig. 4. Note that our results cannot be readily used to directly extract a size effect on flow strength as in (4) because of the stochastic variations in initial yield strength that we found.

5   CONCLUDING REMARKS

Plastic flow in monolithic materials with a single slip system leads to easy glide with no apparent hardening in our simulations. This is to be attributed mainly to the fact that the density of obstacles remains constant during the deformation process, which eventually leads to localization of dislocation activity in 'planar arrays'.

In a material with reinforcing particles, this mechanism is suppressed when the particle size and density is such that all slip planes are blocked by particles. For the morphology studied in Sec. 4, the near-linear hardening is the result of both dislocation-dislocation interactions and the interactions between particles and dislocations; but these effects are not easily separated. There is also no clear distinction between those dislocations that are geometrically necessary and those that are statistically stored. Nevertheless, the former do play a central role and are primarily responsible for the size effect seen here in the hardening of composite materials. Simulations using a different morphology with the same dislocation density but with square particles (as in [7]) did not show a size effect, due to the fact that veins of matrix material remain that allow localization of plastic flow to take place in a similar manner to what is found for the monophase material.

References

[1] Ashby M.F., *Phil. Mag.* **21** (1970) 399–424.

[2] Brown L.M. and Stobbs W.M., *Phil. Mag.* **34** (1976) 351.

[3] Rhee M., Hirth J.P. and Zbib H.M., *Acta Metall. Mater.* **42** (1994) 2645–2655.

[4] Shen Y.-L., Finot M., Needleman A. and Suresh S., *Acta Metall. Mater.* **43** (1995) 1701–1722.

[5] Van der Giessen E. and Needleman A., "On the solution of 2-D plasticity problems with discrete dislocations," Computational Material Modeling, ASME AD–Vol. 42/PVP–Vol. 294, A.K. Noor and A. Needleman Eds. (ASME, New York, 1994) pp. 53–70.

[6] Van der Giessen E. and Needleman A., *Modelling Simul. Mater. Sci. Eng.* **3** (1995) 689–735.

[7] Cleveringa H.H.M., Van der Giessen E. and Needleman A., *Acta Mat.* (1997) in print.

[8] Lubarda V., Blume J.A. and Needleman A., *Acta Metall. Mater.* **41** (1993) 625–642.

[9] Nabarro F.R.N., Theory of Crystal Dislocations (Oxford Univ. Press, Oxford, 1967).

[10] Hirth J.P. and Lothe J., Theory of Dislocations (McGraw–Hill, New York, 1968).

[11] Kubin L.P., Canova G., Condat M., Devincre B., Pontikis V. and Bréchet Y., *Solid State Phenomena* **23** & **24** (1992) 455–472.